Journal of Catalysis 260 (2008) 119–127

Contents lists available at ScienceDirect

Journal of Catalysis

www.elsevier.com/locate/jcat

Preparation of hydrotreating catalysts via an oxalic acid-assisted hydrothermal deposition method

Hao Wang [a,b], Yu Fan [b], Gang Shi [b], Haiyan Liu [b], Xiaojun Bao [a,b,*]

[a] State Key Laboratory of Heavy Oil Processing, China University of Petroleum, Changping, Beijing 102249, PR China
[b] The Key Laboratory of Catalysis, China National Petroleum Corporation, China University of Petroleum, Changping, Beijing 102249, PR China

ARTICLE INFO

Article history:
Received 24 June 2008
Revised 8 September 2008
Accepted 11 September 2008
Available online 9 October 2008

Keywords:
Oxalic acid
Hydrothermal deposition method
Dispersion
Metal–support interaction
Hydrodesulfurization catalyst

ABSTRACT

An oxalic acid-assisted hydrothermal deposition method to prepare highly dispersed W/γ-Al_2O_3 and NiW/γ-Al_2O_3 hydrodesulfurization catalysts without strengthening the metal–support interaction was developed and compared with the conventional impregnation method. The resulting oxidic and sulfided catalysts were characterized, and their catalytic performance was assessed. The results showed that the oxalic acid-assisted hydrothermal deposition method can better disperse tungsten oxide on γ-Al_2O_3 while decreasing the metal–support interaction, resulting in more efficient sulfidation of tungsten oxide and formation of highly stacked WS_2 slabs with short length, and thereby the significantly enhanced hydrodesulfurization activity of the resulting catalysts. The improved dispersion of W species is attributed to the anti-aggregation effect of the oxalic acid adsorbed on active metal particles formed during the hydrothermal deposition process, whereas the strong interaction between carboxyl groups of oxalic acid and hydroxyl groups or unsaturated Al^{3+} on alumina surface accounts for the weakened metal–support interaction.

1. Introduction

Hydrodesulfurization (HDS) is the most widely used technique to remove sulfur from petroleum and petroleum products in the refining industry, and now it is becoming more important because of the increasingly stringent environmental regulations on transportation fuels over the world. As the most important type of HDS catalysts, alumina-supported Mo or W catalysts in which Co and Ni are usually used as promoting elements have been used in the refining industry for more than half a century [1]. Numerous results documented in the literature have shown that, in addition to the local composition, the size and structure of active species particles can significantly affect the catalytic activity and selectivity of supported metal catalysts [2,3]. It is generally agreed that for supported metal catalysts, highly dispersed active species can provide more active sites and thus confer the resulting catalysts with higher catalytic activity [4]. Extensive research [2,5–7] has shown that there are at least two types of "Co(Ni)–Mo(W)–S" phases in alumina-supported (Co)Mo or (Ni)W sulfide catalysts. The type I phase is not fully sulfided and is less stacked, containing some Mo(W)–O–Al linkages with the alumina support related to the strong interaction between Mo(W) and hydroxyl groups on the alumina surface and thus having lower activity. The type II phase is fully sulfided and highly stacked, exhibiting only the weak van der Waals interaction with alumina and thus showing higher activity. For this reason, increasing the dispersion of active metal sulfides while controlling the metal–support interaction is an effective way to enhance the catalytic activity of metal sulfide hydrotreating catalysts [8]. But most of the methods for increasing the dispersion of active species involve strengthening the interaction between active species and support [9,10] and thus are disadvantageous for the formation of a highly stacked type II metal sulfide phase that favors the adsorption and HDS of alkyl-substituted dibenzothiophenes (DBTs), such as 4,6-dimethyldibenzothiophene (4,6-DMDBT), through the prehydrogenation pathways, because the HDS of DBT derivatives with larger molecule size is a geometrically demanding reaction [11,12]. By introducing some chelating agents, such as ethylenediaminetetraacetic acid (EDTA), nitrilotriacetic acid (NTA), and 1,2-cyclohexanediamine-*N*,*N*,*N*,*N*-tetraacetic acid (CyNTA) [13–15], or modification elements, such as phosphorous and fluorine [16–19], the metal–alumina interaction can be weakened, and more stacked metal sulfides can be generated. Nevertheless, this gives rise to the formation of larger active particles and thus poorer dispersion of active species, decreasing the number of active sites and thus being unfavorable for less geometrically demanding reactions like the HDS of smaller sulfide molecules, as pointed out by Sun et al. [12]. In summary, the preparation of alumina-supported metal sulfide hydrotreating catalysts with higher metal dispersion and weaker metal–alumina interaction remains a great challenge.

* Corresponding author. Fax: +86 10 89734979.
E-mail address: baoxj@cup.edu.cn (X. Bao).

0021-9517/$ – see front matter
doi:10.1016/j.jcat.2008.09.010

Herein, we report an oxalic acid assisted-hydrothermal deposition (OHD) method for preparing highly dispersed W/γ-Al_2O_3 and NiW/γ-Al_2O_3 HDS catalysts without strengthening the metal–support interaction. It is well known that for making nanosized metal oxides, aqueous solutions under hydrothermal conditions can offer some advantages over traditional synthesis methods, especially the precise control of the size and shape of the nanophase because of the special reactivity [20–22] and the uniform dispersion of the resulting nanoparticles because of the decreased solution viscosity and low resistance to mass transfer. These two advantages make the OHD method ideally suited for preparing supported metal catalysts with controllable size and dispersion. Moreover, during the hydrothermal deposition process, an organic acid, oxalic acid, was introduced to interact with the hydroxyl groups or unsaturated Al^{3+} on the alumina surface and thereby weaken the metal–support interaction. The combined use of the hydrothermal deposition method and the introduction of an organic acid was expected to yield a catalyst with higher metal dispersion and weaker metal–support interaction. To the best of our knowledge, this method has not yet been reported in open literature.

2. Experimental

2.1. Catalyst preparation

Two W/γ-Al_2O_3 catalysts, designated catalysts OHD and IM, with the same WO_3 loading were prepared by the OHD proposed in this investigation and the conventional pore volume impregnation method (IM), respectively. The OHD involves the following steps. First, 3.0 g of γ-Al_2O_3 particles (20–40 mesh; Sasol GmbH, Germany) were placed in a Teflon-lined stainless-steel autoclave containing 38.6 mL of a 0.1 M sodium tungstate solution. Second, 3.2 mL of a 2.4 M HCl solution was added dropwise to the above solution, after which 9.7 mL of a 0.8 M oxalic acid solution was added dropwise under stirring. Third, the resulting suspension was stirred and heated at 150 °C for 12 h. Finally, the product thus obtained was filtered, washed with deionized water, dried at 110 °C for 2 h, and calcined at 550 °C for 4 h. The IM catalyst was prepared by the IM using ammonium metatungstate as the precursor. The γ-Al_2O_3 support was impregnated with an aqueous solution of ammonium metatungstate for 24 h, dried at 110 °C for 2 h, and finally calcined at 550 °C for 4 h. The WO_3 loading of the two W/Al_2O_3 catalysts determined by X-ray fluorescence spectroscopy (XRF) was 23 wt%.

Two bimetallic NiW/γ-Al_2O_3 catalysts were prepared by two different methods. One catalyst was made by depositing W species on γ-Al_2O_3 extrudates (1.5 mm diameter, 4–5 mm long; Sasol GmbH) through the OHD, and then impregnating Ni species through the IM using nickel nitrate as the precursor. After each step, the extrudates were dried at 110 °C for 2 h and calcined at 550 °C for 4 h to obtain the oxidic NiW/γ-Al_2O_3 catalyst, designated catalyst NiW-OHD. The other catalyst, designated NiW-IM, was prepared by the sequential pore volume impregnation method using aqueous solutions of ammonium metatungstate and nickel nitrate, with W impregnated first, followed by Ni. After each of the above impregnation steps, the extrudates were dried and calcined under the identical conditions used for catalyst NiW-OHD. The WO_3 and NiO loadings of the two NiW/Al_2O_3 catalysts determined by XRF were 23 and 2.6 wt%, respectively.

2.2. Characterization

The catalysts' WO_3 and NiO contents were determined by XRF conducted on a Rigaku ZSX-100e instrument. X-ray diffraction (XRD) analyses were conducted on a Shimadzu XRD-6000 diffractometer using Cu$K\alpha$ radiation and operating at 40 kV and 30 mA with 2θ scanning speed at 4°/min and diffraction lines of 2θ between 10° and 80°.

Temperature-programmed reduction (TPR) analyses of the oxidic catalysts were performed on a home-built apparatus. Before reduction, the catalyst sample to be measured (each 0.1 g) was pretreated in an Ar stream at 450 °C for 2 h and then cooled to room temperature. Then the Ar flow was switched to a 10 v% H_2/Ar flow, and the catalyst sample was heated to 1050 °C at a rate of 10 °C/min and then kept at this temperature for 0.5 h. The H_2 consumption for the reduction of the corresponding metal oxide in the catalyst was detected by a thermal conductivity detector (TCD).

Nitrogen adsorption–desorption measurements of the catalysts were performed on a Micromeritics ASAP 2002 adsorption instrument. The sample was degassed in a preparation station at 250 °C and in a vacuum of 10^{-5} Torr for 15 h, then switched to the analysis station for adsorption–desorption at liquid nitrogen temperature. The specific surface areas and pore volumes of the catalysts were calculated from N_2 adsorption–desorption isotherms using the BET and BJH methods [23].

Fourier transformed infrared spectroscopy (FTIR) measurements were performed on a Thermal Nicolet 560 IR spectrophotometer. Three samples were prepared: oxalic acid, γ-Al_2O_3, and γ-Al_2O_3 impregnated with oxalic acid. The latter sample was prepared by impregnating γ-Al_2O_3 with a 0.8 M oxalic acid solution through the pore volume impregnation method and drying at 110 °C for 6 h. Before measurement, all of the samples were crushed to powder and dried at 110 °C. The IR spectra of the samples were recorded in the wavenumber range of 400 to 4000 cm^{-1}. All of the spectra were calculated from 64 scans at a 0.35 cm^{-1} resolution.

High-resolution transmission electron microscopy (HRTEM) images of the sulfided catalysts were obtained on a Philips Tecnai G2 F20 transmission electron microscope operated at an accelerating voltage of 200 kV. The catalysts were sulfided with a 3 wt% CS_2/cyclohexane mixture at 400 °C and 4 MPa for 4 h and kept in cyclohexane before measurement. To quantitatively compare the stacking layer numbers and lengths of the metal sulfide slabs on the catalysts prepared by the different methods, about 20 representative micrographs involving 500–700 sulfide slabs were obtained from different parts of each catalyst, and statistical analyses were carried out [24,25].

X-ray photoelectron spectroscopy (XPS) measurements of the oxidic catalysts and the corresponding sulfide catalysts were performed on a VG ESCA Lab 250 spectrometer using Al$K\alpha$ radiation. Before measurement, the oxidic catalysts were crushed to powder. The sulfide catalysts were analyzed according to the following procedure. The oxidic catalysts were first sulfided in a mixture of 3 wt% CS_2/cyclohexane at 400 °C and 4 MPa for 4 h. Then the catalysts were cooled to room temperature in a nitrogen flow, ground, and kept in cyclohexane to prevent oxidation. Before the XPS measurements, the samples were pressed onto a stainless steel sample holder in air; the holder was immediately mounted onto the XPS machine. The Al2p peak at 74.6 eV was used as an internal standard to compensate for sample charging. To quantify the contents of W^{4+} and W^{6+} species, the XPS spectra obtained were fitted using XPSPEAK version 4.1 software [7]. A Shirley background was applied, and the W4f spectra were deconvoluted by fitting the experimental spectra to a mixed Gaussian–Lorentzian function, with the Lorentzian function taking a fraction of 70 to 80% [16,17].

2.3. HDS performance assessment

The DBT HDS activity of the W/Al_2O_3 and NiW/Al_2O_3 catalysts was assessed in a fixed-bed microreactor using 1 wt% DBT in cyclohexane as a model compound. The catalyst (2 mL) to be assessed

was diluted with quartz particles of the same volume and mean size. Before the reaction, the catalysts were presulfided for 4 h at 360 °C, total pressure 4.0 MPa, and a H_2/hydrocarbon (HC, 3 wt.% CS_2 in cyclohexane) volumetric ratio of 300. The HDS reaction was carried out under the conditions of 360 °C, a liquid volume hourly space velocity (LHSV) of 8.0 h^{-1}, total pressure of 4.0 MPa, and a H_2/HC volumetric ratio of 400. After steady state was reached, the liquid product was collected, and the sulfur contents in the reactant and product were analyzed by a Jiangfen Instruments WK-2C microcoulometer. Assuming a pseudo-first-order reaction for the DBT HDS, the catalyst activity of the two catalysts was expressed by the following equation [26,27]:

$$k = \frac{F}{m}\ln\left(\frac{1}{1-x}\right),$$

where x is the HDS conversion of DBT, F is the molar feed rate of DBT in mol s^{-1}, m is the catalyst mass in grams, and k is the rate constant of HDS. In addition, the DBT HDS rate was calculated in terms of turnover frequency, TOF (h^{-1}), defined as the number of desulfurized DBT molecules per hour and per catalytic site (per W atom) [8,28].

The HDS behavior of the two NiW/Al_2O_3 catalysts also was evaluated using a fluid catalytic cracking (FCC) diesel from a Chinese refinery with its boiling point in the range of 201 to 412 °C, a density of 0.8943 g cm^{-3}, and a sulfur content of 1421 ppm. The HDS reaction was conducted in the same fixed-bed microreactor used for the DBT HDS. Before being loaded into the reactor, 2 mL of the catalyst to be tested was diluted with the same volume of quartz particles. The two NiW/Al_2O_3 catalysts were sulfided in a mixture of 3 wt% CS_2 in cyclohexane. The sulfidation procedure comprised the following steps: (1) the sulfiding feed was introduced to wet the catalyst bed at 150 °C and 6 MPa, after which the bed temperature was linearly increased to 180 °C at a rate of 60 °C/h and kept at this temperature for 0.5 h; (2) the bed temperature was increased to 230 °C at a rate of 60 °C/h and maintained there for 2 h; (3) the bed temperature was increased to 280 °C at the same rate and maintained there for 0.5 h; and (4) the bed temperature was increased to the final sulfidation temperature 360 °C, and the operation was stabilized for 3 h. After sulfidation, the feeding flow was switched to the diesel feed, and the HDS assessment was carried out. The operating conditions were LHSV, 1.5 h^{-1}; 360 °C; total pressure, 6 MPa; and a H_2/oil volume ratio of 500. After steady state was achieved, the liquid product was sampled for analysis. The HDS activity of the two NiW/Al_2O_3 catalysts for the FCC diesel HDS was expressed in terms of the rate constant, expressed by

$$k = \frac{W_L}{m}\frac{1}{n-1}\left[\frac{1}{S_P^{n-1}} - \frac{1}{S_f^{n-1}}\right],$$

where k (h^{-1} $(ppm)^{1-n}$) is the apparent rate constant for the conversion of sulfur present in the FCC diesel, n is the order of the reaction, W_L (g h^{-1}) is the FCC diesel flow rate, m (g) is the catalyst mass, S_p (ppm) is the total sulfur content of the product, and S_f (ppm) is the total sulfur content of the feedstock [29,30]. In the present study, n is 1.65 [31].

3. Results and discussion

3.1. Characterization of the oxidic W/γ-Al_2O_3 catalysts

3.1.1. XRD and XPS

The XRD patterns of the two oxidic W/γ-Al_2O_3 catalysts and the γ-Al_2O_3 support are shown in Fig. 1. Whereas all of the samples show peaks at $2\theta = 37.2°$, 45.9°, and 66.8°, ascribed to the support γ-Al_2O_3 (PDF No. 29-1486), only catalyst IM shows peaks

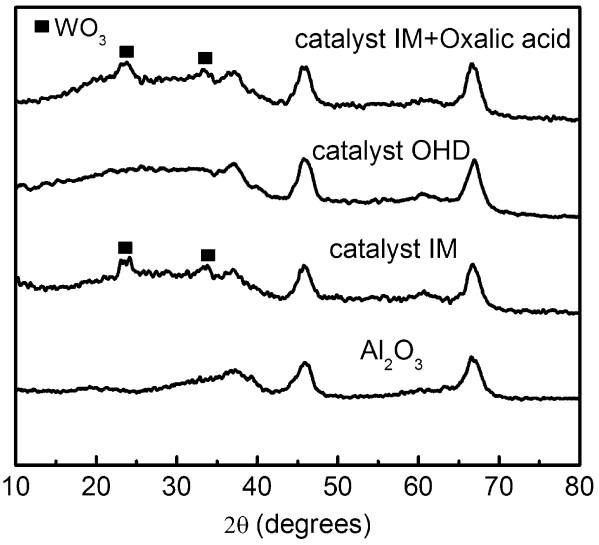

Fig. 1. XRD patterns of Al_2O_3 and catalysts IM, OHD, and IM + oxalic acid.

at $2\theta = 23.1°$, 23.6°, 24.4°, and 33°, corresponding to bulk WO_3 crystallites (PDF No. 43-1035), signifying that larger WO_3 particles were formed on the surface of γ-Al_2O_3 [32,33]. This finding is similar to those of Karakonstantis et al. [34], who observed crystalline WO_3 on a W/Al_2O_3 catalyst loaded with 21.2 wt% WO_3 prepared by IM. In contrast, no peaks corresponding to bulk WO_3 crystallites are seen in the XRD pattern of catalyst OHD, indicating that WO_3 is highly dispersed on the support [35]. The smaller peak at $2\theta = 60.9°$ for both W/Al_2O_3 catalysts may be attributed to the trace amount of sodium tungsten oxide (PDF No. 05-0247) impurities.

XPS can be a useful tool for studying the dispersion of active metals in supported catalysts. The surface atomic ratios of active metal elements to the aluminum element in the alumina support determined by XPS can be used as a measure of the coverage of active metals in alumina-supported hydrotreating catalysts [28,30]. Thus, the W/Al atom ratios on the two oxidic W/γ-Al_2O_3 catalysts were measured by XPS in the present investigation; the results are given in Table 1. It can be seen that the W/Al ratio on catalyst OHD is higher than that on catalyst IM, even though the two catalysts have the same WO_3 content, as determined by XRF. This indicates that the former catalyst has greater WO_3 dispersion.

During the IM process, the deposition of active species often occurs, due to the uncontrollable evaporation of the impregnating solution and the decomposition of the metal salt precursor in the drying and calcination steps, leading to the inhomogeneous distribution or even the greater crystallite formation of active species on support surface. This gives rise to the decreased dispersion of active species in the resulting catalysts [10,36,37].

In the conventional precipitation method for preparing supported metal catalysts, active species are formed through the precipitating reaction between an active metal salt precursor and a precipitating agent. The main drawback of this method is that the resulting active particles are larger and thus can hardly diffuse into the support, leading to decreased dispersion of active species [36].

For the OHD proposed in the present investigation, the formation of the tungsten oxide active species occurs through hydrothermal deposition rather than through decomposition of the metal salt precursor in the calcinations step. Distinctly different from the conventional precipitation process, the OHD that we have developed can significantly promote the dispersion of WO_3 because of the following properties:

Table 1
Typical properties and DBT HDS activity of the W/Al_2O_3 catalysts.

	BET specific surface area ($m^2\,g^{-1}$)	Pore volume ($cm^3\,g^{-1}$)	W/Al	HDS rate constant (10^{-4} mol $g^{-1}\,h^{-1}$)	TOF (h^{-1})
Al_2O_3	206	0.49	–	–	–
Catalyst IM	180	0.38	0.054	4.13	0.27
Catalyst OHD	199	0.44	0.086	6.64	0.38

(1) The decreased viscosity of the aqueous solution under the hydrothermal conditions greatly benefits the diffusion of the reacting species into the support pore channels, leading to improved distribution of the active species particles formed on the surface and in the pore channels of the support.
(2) The use of oxalic acid in the hydrothermal deposition system results in hydrogen bonding between the carboxyl groups of oxalic acid and the $(WO_n)^-$ anions adsorbed on the surfaces of the resulting WO_3 particles. This hydrogen bonding separates WO_3 particles from one another and prevents their aggregation to form larger crystallites [38].
(3) The dispersant oxalic acid also plays an important role in preventing the aggregation of WO_3 particles during the subsequent drying and calcination steps. First, oxalic acid used as an additive with lower surface tension than water [38,39] can adsorb on the WO_3 particles and thus decrease the capillary forces between WO_3 particles and restrain the aggregation of WO_3 particles during the drying step [40]. Second, as a chelating agent, oxalic acid can coordinate with tungstic acid to slow down the growth of tungstic acid particles, and its presence during the calcination step can inhibit particle sintering, as reported by Lu et al. [41]. Third, during the calcination step, the decomposition of oxalic acid releases CO_2 and H_2O, which separate the WO_3 particles and prevent their aggregation [42]. Several researchers also found that adding surfactants or organic complexing agents as dispersants could effectively inhibit the growth of nanoparticles synthesized, even though these organic materials were removed in the thermal treatment [43–45].

To gain insight into the promoting effects of the hydrothermal deposition environment on the dispersion of WO_3, two more W/Al_2O_3 catalysts were prepared. The first (denoted as catalyst IM + Oxalic acid) was made by adding the same amount of oxalic acid used for preparing catalyst OHD into the impregnation solution for preparing catalyst IM. The second was prepared at room temperature and ambient pressure using the same preparation system for catalyst OHD. The XRD characterization results (Fig. 1) reveal formation of bulk WO_3 crystallites on the former catalyst, indicating that oxalic acid cannot improve the dispersion of WO_3 when used in the IM. This may be due to the decomposition of oxalic acid during calcination before the formation of WO_3, because oxalic acid has a decomposition temperature of 175 °C, much lower than the 350 °C of metatungstate, whereas WO_3 particles are formed directly in the OHD process. In contrast, the XRF analysis results show that the latter W/Al_2O_3 catalyst contains only 11.3 wt% WO_3, much lower than the 23 wt% of catalyst OHD, resulting from the precipitation reaction between tungstate and hydrochloric acid deposited on the alumina. This suggests that the reduced viscosity of the hydrothermal solution can increase the mobility of the reactants and thereby enhance their diffusion into the pore channels of the support. As a result, numerous active particles are deposited on the support uniformly. Shin et al. [46] also found that solvents with lower viscosity and high diffusivity were favorable for the delivery of organic functionalized molecules to the inner surface of microporous materials.

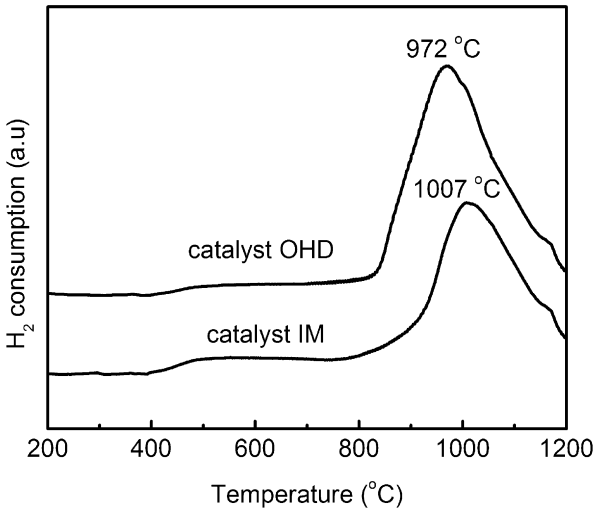

Fig. 2. TPR profiles of catalysts IM and OHD.

3.1.2. N_2 adsorption–desorption

The pore volumes and BET surface areas of the two W/Al_2O_3 catalysts introduced in Section 3.1.1 are listed in Table 1. It can be seen that catalyst OHD has a greater specific surface area and pore volume than catalyst IM. This is because the IM yields larger WO_3 crystallites, which cause the plugging or even complete closure of the support pore channels and thereby decrease the catalyst specific surface area and pore volume, as reported previously [10], whereas OHD produces smaller WO_3 crystallites that affect the pore structure of the resulting catalyst only slightly. This viewpoint also is supported by the HRTEM characterization results presented below.

3.1.3. TPR

To obtain information on the metal–support interaction, the TPR profiles of catalysts OHD and IM were measured. The results, shown in Fig. 2, show that for catalysts OHD and IM, the maximum reduction peaks assigned to the reduction of the oxidic tungsten species are located at 972 and 1007 °C, respectively, illustrating the weaker interaction between the oxidic tungsten species and alumina in catalyst OHD compared with catalyst IM. The weaker metal–support interaction greatly benefits the sulfidation of the oxidic tungsten species [16], as further confirmed by the XPS characterization results for the corresponding sulfided W/Al_2O_3 catalysts.

3.1.4. FTIR

To gain further insight into the role of oxalic acid in the OHD process, the interaction between oxalic acid and γ-Al_2O_3 was studied by impregnating γ-Al_2O_3 with the same amount of the oxalic acid solution used for preparing catalyst OHD. Fig. 3 shows the FTIR spectra of γ-Al_2O_3, γ-Al_2O_3 impregnated with oxalic acid, and oxalic acid. The strong absorbance bands in the wavenumber ranges of 1750–1650 cm^{-1} and 1350–1250 cm^{-1} are associated with the C=O and C–O bonds of the carboxyl groups in carboxylic acid [47], and these two bands are found for both γ-Al_2O_3 impregnated with oxalic acid (1700 and 1294 cm^{-1}) and oxalic acid

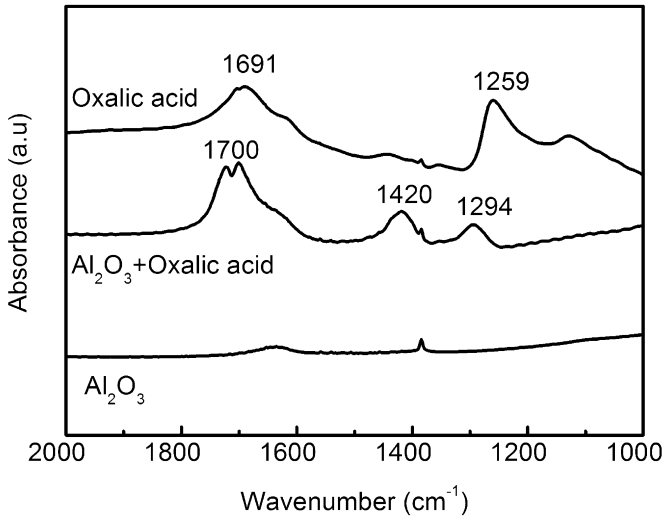

Fig. 3. IR spectra of γ-Al_2O_3, γ-Al_2O_3 impregnated with oxalic acid, and oxalic acid samples.

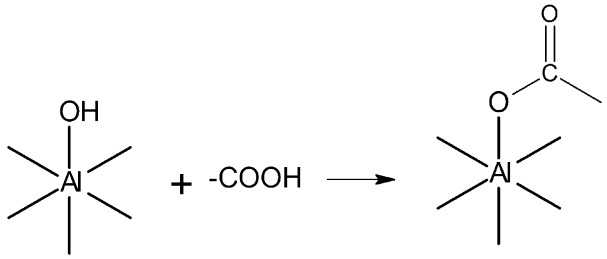

Scheme 1. Reaction between the alumina support and the carboxyl groups of oxalic acid.

(1691 and 1259 cm^{-1}). For γ-Al_2O_3 impregnated with oxalic acid, a strong peak appears at about 1420 cm^{-1} that is typical for the symmetric $-COO^-$ stretching of carboxylate species [47]. This peak was not observed for the γ-Al_2O_3 and oxalic acid samples, however. These results suggest that the carboxyl groups of oxalic acid can react with the surface hydroxyl groups of γ-Al_2O_3 to form a carboxylate-like structure, in good agreement with previous findings [48]. The reaction between the alumina support and the carboxyl groups of oxalic acid can be illustrated by Scheme 1. Dobson and McQuillan [47] found that on the surfaces of metal oxides, such as TiO_2 and Al_2O_3, carboxylic acid adsorption occurs, because carboxyl groups can act as a ligand to be anchored onto the vacant coordination sites of surface metal ions. Therefore, the possibility that the carboxyl groups of oxalic acid interact with the coordinatively unsaturated Al^{3+} sites on the surface of γ-Al_2O_3 to form carboxylate cannot be excluded. Evans and Weinberg [49] suggested that adsorbed carboxylic acids might interact with alumina surface by sharing a hydrogen atom between an oxygen atom in the carboxylic group and an oxygen atom on the alumina surface through strong hydrogen bonding. For various organic compounds, the adsorption of carboxylic acids on alumina is very strong because of their much higher adsorption energies compared with those of others [48]. Moreover, compared with the mono-carboxylic acids, the presence of the second carboxyl group in aliphatic dicarboxylic acids, such as oxalic acid, allows the formation of more stable surface structures on the surfaces of metal oxides [47].

In the IM process, the hydroxyl groups and coordinatively unsaturated Al^{3+} existing on the surface of alumina strongly interact with the tungstate precursor. This leads to a strong metal–support interaction and, consequently, poorer sulfidation of WO_3 species and less formation of highly active type II WS_2 phase [12]. In the

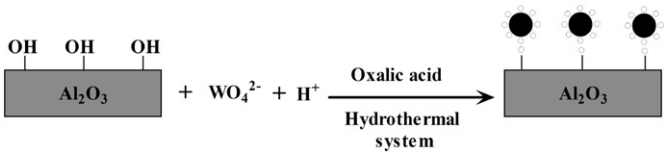

Scheme 2. Suggested scheme of the oxalic acid (white balls)-assisted hydrothermal deposition of WO_3 (black balls).

OHD process, however, the carboxyl groups of oxalic acid interact with the hydroxyl groups or coordinatively unsaturated Al^{3+} sites on the surface of γ-Al_2O_3, resulting in the formation of a layer between the metal precursor and alumina surface [50], thereby preventing the formation of strong metal–support bonding in catalyst OHD.

In summary, the deposition of WO_3 on alumina in the OHD process can be described by Scheme 2. WO_3 particles are formed through the precipitation reaction between tungstate and HCl under hydrothermal conditions, and oxalic acid added as a dispersant adsorbs on the WO_3 particles through H-bonding interactions between the carboxyl groups of oxalic acid and negatively charged WO_3 particles. The lower viscosity of the OHD system facilitates diffusion of the precursor into the pore channels of the support, thereby resulting in the homogeneous deposition of WO_3. The formation of a carboxylate-like layer on the support surface due to the interaction of oxalic acid with the surface hydroxyl groups of alumina inhibits the strong interaction between WO_3 and alumina. In the subsequent drying step, the oxalic acid (with lower surface tension) can decrease the capillary force between WO_3 particles and thus prevent their aggregation. In the final calcination step, the coordination of oxalic acid that acts as a ligand with tungstic acid can minimize the sintering of WO_3 particles, and the gases produced by the decomposition of oxalic acid can separate the particles to protect them from aggregation. All the effects result in higher metal dispersion and weaker metal–support interactions in catalyst OHD.

3.2. Characterization of the sulfided W/γ-Al_2O_3 catalysts

3.2.1. HRTEM

HRTEM is a powerful, indispensable technique for studying the morphology of active phases that has been widely applied in the study of sulfide catalysts [25]. The particle size of the active phase is considered indicative of the dispersion of supported metal sulfides [24]. For this reason, the morphology of catalysts IM and OHD after sulfidation was observed by HRTEM; representative HRTEM images are shown in Fig. 4. To make a quantitative comparison, a statistical analysis was conducted of 500 to 700 sulfide slabs from about 20 micrographs obtained from different parts of each sample [25]. Table 2 gives the slab length distributions and stacking layer number distributions of the two catalysts. It can be seen that the OHD significantly decreases the fraction of the WS_2 slabs larger than 5 nm, with the average length of the WS_2 slabs decreasing from 6.1 nm for catalyst IM to 4.8 nm for catalyst OHD. This indicates that the dispersion of the active-phase WS_2 is greater on catalyst OHD than on catalyst IM. Both the XRD characterization results of the oxidic catalysts and the HRTEM characterization results of the corresponding sulfided catalysts suggest that the dispersion of the oxidic W species is directly related to that of their derived WS_2 species, as has been reported by Usman et al. [51] and Okamoto et al. [52] for oxidic and sulfided Mo/Al_2O_3 catalysts.

As shown in Table 2, the WS_2 slabs on catalyst OHD also are more stacked than those on catalyst IM, with the average stacking layer number of the WS_2 slabs increasing from 1.4 on catalyst IM to 1.6 on catalyst OHD. The highly stacked WS_2 slabs on catalyst OHD are attributed to the weaker metal–support interaction, be-

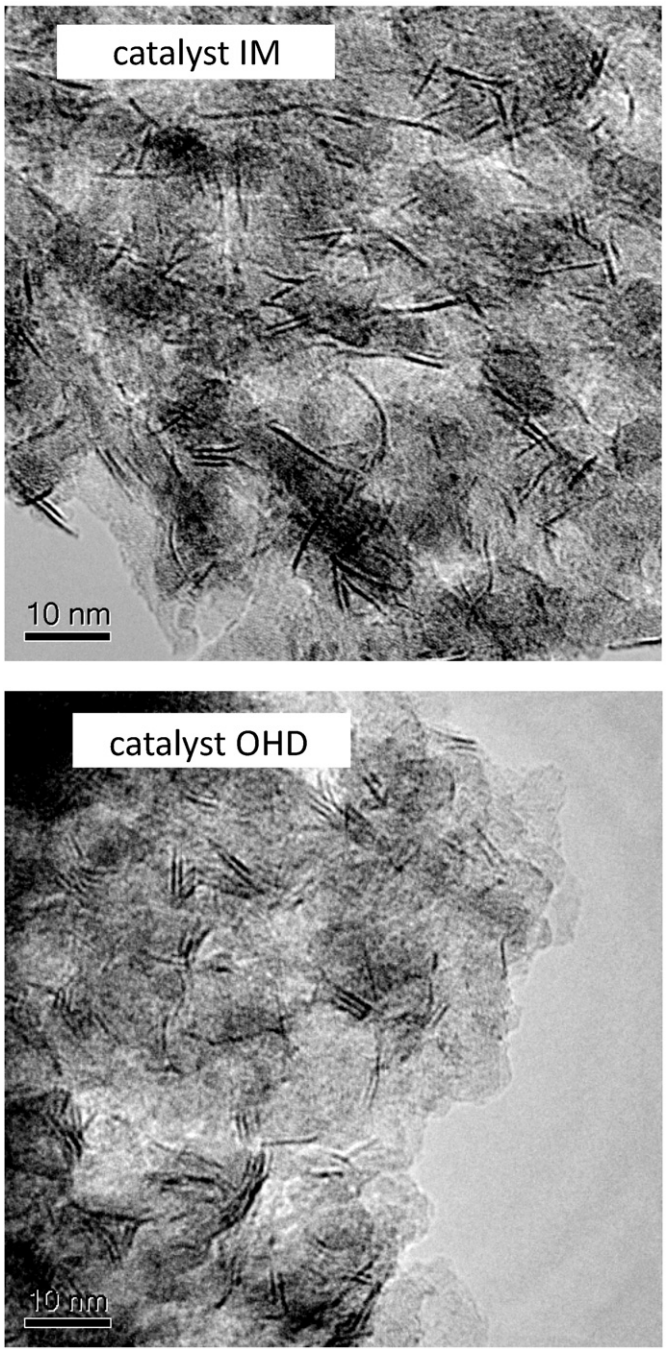

Fig. 4. HRTEM images of sulfided catalysts IM and OHD.

cause weaker support–O–WS_2 bonds can be more easily cleaved, and thus highly stacked WS_2 particles are formed [8]. Here we must point out that the bulk WO_3 crystallites formed on catalyst IM do not increase the stacking layers of WS_2, because the decreased dispersion of WO_3 mainly increases the length of the WS_2 slabs and does not increase the stacking degree of WS_2 slabs under normal sulfidation conditions, as described by Bentiez et al. [53] and Ramírez et al. [54].

3.2.2. XPS

The sulfidation degree of the oxidic active species is a key parameter affecting the catalytic activity of Mo- and W-based hydrotreating catalysts [2]. To elucidate the effect of the preparation methods on the sulfidation behavior of the resulting oxidic catalysts, XPS was used to study the sulfidation degree of the oxidic

Table 2
Length and stacking layer number distributions of the WS_2 slabs over the sulfided catalysts IM and OHD.

	Frequency (%)	
	Catalyst IM	Catalyst OHD
Length (nm)		
<3	3.4	12.8
3–4	10.9	29.7
4–5	20.9	23.5
5–6	21.9	13.4
6–8	27.7	12.8
>8	15.2	7.8
Stacking layer number		
1	71.8	55.9
2	22.1	34.6
3	5.2	7.8
>3	0.9	1.7

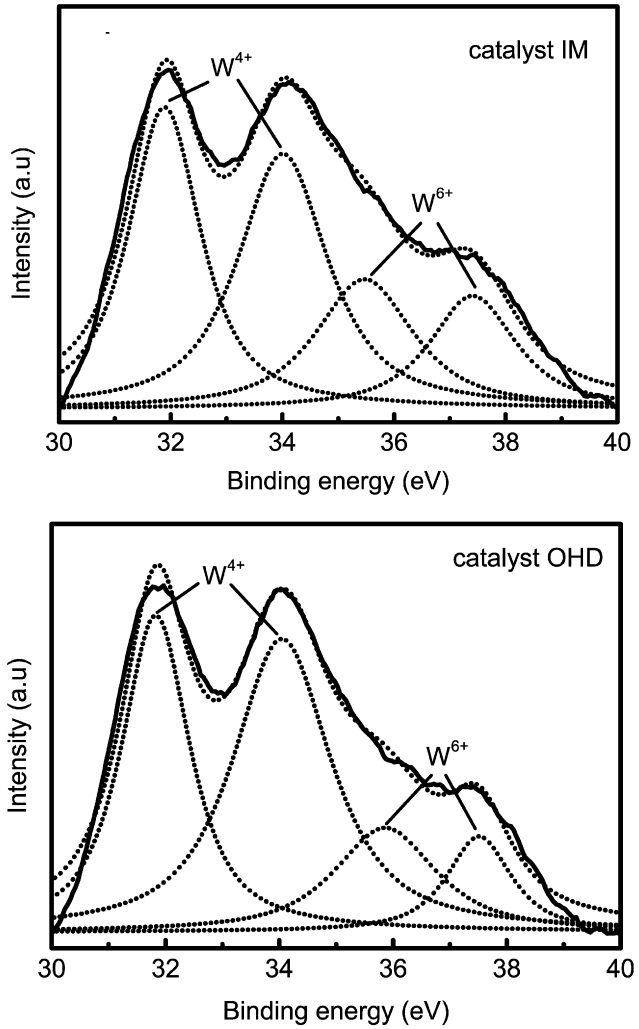

Fig. 5. W4f XPS spectra of the sulfided catalysts IM and OHD.

W species on catalysts IM and OHD. Fig. 5 shows the W4f XPS spectra of sulfided catalysts IM and OHD and their deconvolution. Each spectrum curve consists of two partially overlapped doublets arising from the $4f_{7/2}$ and $4f_{5/2}$ curves of W^{6+} and W^{4+}, as indicated by their individual peaks obtained by fitting. The binding energies of the $W4f_{7/2}$ and $W4f_{5/2}$ levels for W^{4+} are about 31.9 and 34.0 eV, respectively, and those for W^{6+} are about 35.7 and 37.5 eV [16]. Here the sulfidation degree of the oxidic W species,

$W_{sulfidation}$, is defined as the ratio of W^{4+} (WS_2) to the sum of W^{4+} (WS_2) and W^{6+} (WO_3), that is, $W_{sulfidation} = W^{4+}/(W^{4+} + W^{6+})$ [16,17]. The fitting results show that $W_{sulfidation}$ is 75% for catalyst OHD and 67% for catalyst IM, respectively. Because $W_{sulfidation}$ depends inversely on the W–O–Al linkages, because of the stronger interaction of W with the basic hydroxyl groups on the alumina surface [7], the higher $W_{sulfidation}$ over catalyst OHD can be ascribed to the weaker metal–support interaction. Considering that full sulfidation of oxidic metal species is a prerequisite for the highly active type II WS_2 phase [7], catalyst OHD would be expected to be more active than catalyst IM after sulfidation.

3.3. HDS activity of the W/γ-Al_2O_3 catalysts

The DBT HDS performance of the two sulfided W/Al_2O_3 catalysts was assessed. The results, given in Table 1, show that both the HDS rate constant and TOF obtained over catalyst OHD are higher than those obtained over catalyst IM. The enhanced HDS activity of catalyst OHD can be interpreted in the following manner. First, the number of active sites is increased over the former, due to the improved dispersion of the active phase. As shown in the HRTEM images, the WS_2 slabs are much shorter in catalyst OHD than in catalyst IM. It is generally agreed that the shorter the WS_2 slabs, the higher the fraction of catalytically active edge planes, and thus the greater the catalyst activity [4,27]. Second, the WO_3 species have a greater sulfidation degree and the resulting WS_2 slabs have higher stacking, due to the decreased metal–support interaction. The increased stacking degree of metal sulfide slabs is beneficial for the adsorption of larger DBT molecules in the planar mode and leads to enhanced DBT HDS activity, as pointed out by Hensen et al. [11]. It is the perfect combination of higher dispersion and high stacking degree that gives the resulting catalyst enhanced activity for both the direct desulfurization (DDS) and hydrogenation (HYD) pathways of DBT HDS, as we have reported previously [55].

3.4. Characterization of the NiW/γ-Al_2O_3 catalysts

In industrial diesel HDS catalysts, Ni and Co usually are introduced as promoters, because the formation of the so-called "Ni(Co)–W(Mo)–S" phase in which Ni atoms are located at the edges of WS_2 layers can produce some synergetic effects [27]. To explore the industrial potential of the OHD developed in the present investigation, two NiW/γ-Al_2O_3 bimetallic catalysts, designated NiW-OHD and NiW-IM, were prepared using the OHD and IM, respectively, and their HDS activities for the DBT model compound and a real FCC diesel feed were tested. In view of the relatively lower Ni loading in industrial HDS catalysts and thus the easier Ni dispersion, Ni was introduced by the IM for both catalysts. For comparison purposes, the WO_3 and NiO loadings of the two catalysts were controlled at 23 and 2.6 wt%, respectively. The Ni/W atomic ratio of the two catalysts was 0.35, considered the optimal value for achieving the best HDS activity [4].

3.4.1. XRD and XPS

Fig. 6 shows XRD patterns of the two oxidic NiW/γ-Al_2O_3 catalysts. It can be seen that these patterns are similar to those of the catalysts without Ni introduction; that is, the peaks at $2\theta = 23°$ and 33° attributed to the crystalline WO_3 are present for catalyst NiW-IM but absent for catalyst NiW-OHD. No peaks ascribed to NiO crystalline are observed for either catalyst, indicating that the introduction of Ni did not affect the dispersion of W species and that NiO was highly dispersed.

The surface W/Al and Ni/Al atomic ratios of the two oxidic NiW catalysts also were measured by XPS. The results, given in Table 3, show that both the surface W/Al and Ni/Al atomic ratios of catalyst NiW-OHD are higher than those of catalyst NiW-IM. On the one hand, the higher surface W/Al atomic ratio can be ascribed to the promoting effect of the OHD process on WO_3 dispersion. On the other hand, the hydrothermal deposition process decreased the number of hydroxyl sites on the surface of alumina, as mentioned in Section 3.1.4, leading to less incorporation of Ni cations into the lattices of alumina and a slightly increased surface Ni/Al atomic ratio of catalyst NiW-OHD.

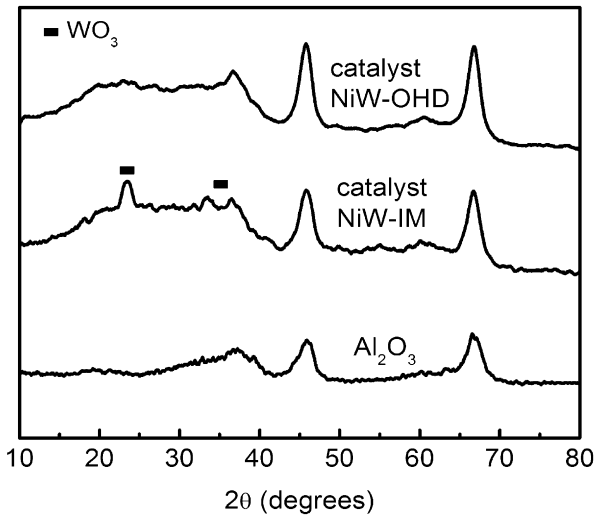

Fig. 6. XRD patterns of γ-Al_2O_3 and catalysts NiW-IM and NiW-OHD.

Table 3
Surface atomic ratios and DBT HDS activity of the NiW/Al_2O_3 catalysts.

	W/Al	Ni/Al	HDS rate constant (10^{-4} mol g^{-1} h^{-1})	TOF (h^{-1})
Al_2O_3	–	–	–	–
NiW-IM	0.047	0.025	5.73	0.30
NiW-OHD	0.070	0.030	12.1	0.41

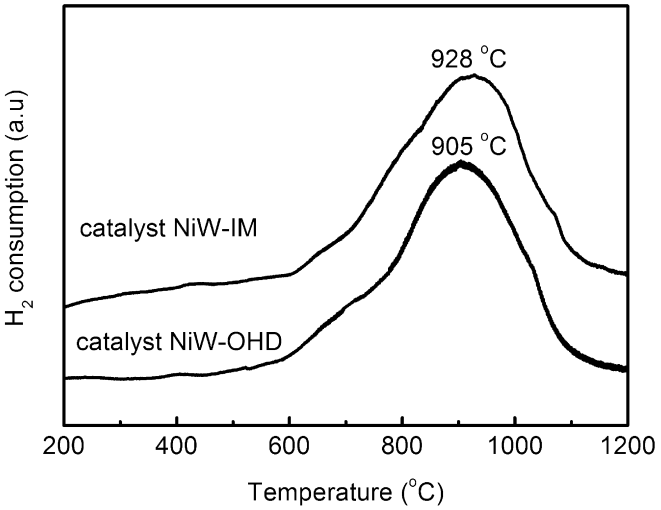

Fig. 7. TPR profiles of catalysts NiW-IM and NiW-OHD.

3.4.2. TPR

The TPR profiles of the oxidic NiW-IM and NiW-OHD catalysts are shown in Fig. 7. Both catalysts have only a single prominent peak at 900–1000 °C, ascribed to reduction of the supported tungsten oxide species. However, the peak temperature for catalyst NiW-IM is 23 °C higher than that for catalyst NiW-OHD, indicating weaker interaction between the tungsten oxide species and

alumina in NiW-OHD. We also note that compared with those of the W/γ-Al_2O_3 catalysts reported earlier, the reduction peaks of the Ni-promoted catalysts shift to low-temperature side, suggesting that the promoter Ni can increase the reducibility of tungsten species [32].

3.5. HDS activity of the NiW/γ-Al_2O_3 catalysts

The DBT HDS rate constants and TOFs of the two NiW catalysts are given in Table 3. The table shows that whereas introduction of the Ni promoter improves the DBT HDS activity of the two catalysts, catalyst NiW-OHD is more active than catalyst NiW-IM for DBT HDS.

The HDS rate constants of catalysts NiW-OHD and NiW-IM calculated from the FCC diesel HDS performance assessment are 0.58 and 0.23 h^{-1} $(ppm)^{-0.65}$, respectively. Setting the volume HDS activity of the NiW-IM catalyst at 100, the relative volume HDS activity of catalyst NiW-OHD is 252. When used in the FCC diesel hydrodesulfurization, catalyst NiW-OHD produces a product containing about 10 ppm sulfur, in full compliance with the sulfur regulations of Euro V diesel. Because the introduction method and content of Ni in the two NiW catalysts are the same, the greater catalytic activity of catalyst NiW-OHD is attributed to the hydrothermal deposition method used for loading W species. On the one hand, the hydrothermal deposition environment used for depositing W is advantageous for the formation and dispersion of uniform WO_3 particles, and the resulting WS_2 slabs with higher dispersion provide more edge sites for the incorporation of Ni atoms to form Ni–W–S active sites [51,56]. On the other hand, the promoter atoms are embedded onto the highly stacked WS_2 slabs; correspondingly, the resulting Ni–W–S active phase also is highly stacked [8]. Both effects favor the adsorption and HDS of alkyl-substituted dibenzothiophenes, such as 4,6-DMDBT, through the prehydrogenation pathways [12,57], and thus enhance the diesel HDS activity of catalyst NiW-OHD.

To compare the diesel HDS activity of the catalyst NiW-OHD with the existing hydrotreating catalysts, a commercial NiW/Al_2O_3 catalyst (kindly provided by Fushun Catalyst Factory, PetroChina Company, Ltd.) loaded with 23 wt% WO_3, 2.6 wt% NiO, and 2.5 wt% F was used as a reference catalyst. The diesel HDS rate constant of the commercial catalyst is 0.24 h^{-1} $(ppm)^{-0.65}$, much lower than that of catalyst NiW-OHD and similar to that of catalyst IM. This result again demonstrates that the OHD developed in the present investigation can improve the HDS activity of the NiW/Al_2O_3 catalyst.

A plausible question that has been raised is whether the weakened metal–support interaction influences the activity stability of the catalyst prepared by the OHD method. To answer this question, 4 mL catalyst of NiW-OHD was assessed under the conditions described above for 500 h. The variation trend of HDS conversion as a function of time on stream is given in Fig. 8. This figure shows that the NiW-OHD has stable HDS activity, with sulfide conversion in the FCC diesel maintained at 99.1–99.3% and the sulfur content in the product maintained at about 10 ppm.

3.6. Conclusion

In the present work, an oxalic acid-assisted hydrothermal deposition method for preparing γ-Al_2O_3-supported W and NiW hydrotreating catalysts was developed. Compared with the conventional impregnation method, this method can better disperse WO_3 species on γ-Al_2O_3 and weaken the metal–support interaction, leading to increased sulfidation of the tungsten oxide species and formation of shorter and more stacked WS_2 slabs and thereby enhanced HDS activity of the resulting catalysts. We have shown that the improved dispersion of W species was attributed to the hydrogen bonding between the oxalic acid and WO_3 particles, and that the weakened metal–support interaction was due to strong interaction of the carboxylic acid groups of oxalic acid with the surface hydroxyl or unsaturated Al^{3+} sites on the alumina support. The oxalic acid-assisted hydrothermal deposition method weakens the dependence of metal dispersion on the metal–support interaction and thus provides a novel way of preparing high-performance supported metal catalysts that have wide application in industry.

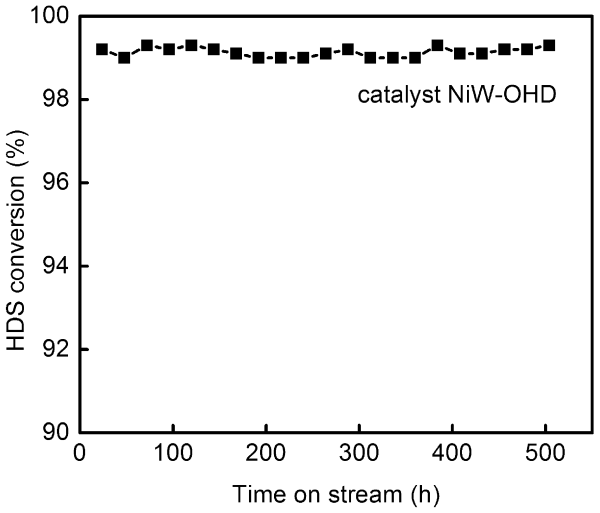

Fig. 8. HDS conversion with time-on-stream over catalyst NiW-OHD.

Acknowledgments

The authors thank the Ministry of Science and Technology of China for providing financial support through the National Basic Research Program (Grant 2004CB217807).

References

[1] C. Song, Catal. Today 86 (2003) 211.
[2] H. Topsøe, B.S. Clausen, Catal. Rev. Sci. Eng. 26 (1984) 395.
[3] M. Daage, R.R. Chianelli, J. Catal. 149 (1994) 414.
[4] L. Vradman, M.V. Landau, M. Herskowitz, V. Ezersky, M. Talianker, S. Nikitenko, Y. Koltypin, A. Gedanken, J. Catal. 213 (2003) 163.
[5] B. Hinnemann, J.K. Nørskov, H. Topsøe, J. Phys. Chem. B 109 (2005) 2245.
[6] H. Topsøe, B. Hinnemann, J.K. Nørskov, J.V. Lauritsen, F. Besenbacher, P.L. Hansen, G. Hytoft, R.G. Egeberg, K.G. Knudsen, Catal. Today 107–108 (2005) 12.
[7] E.J.M. Hensen, V.H.J. de Beer, J.A.R. van Veen, R.A. van Santen, Catal. Lett. 84 (2002) 59.
[8] Usman, T. Kubota, Y. Araki, K. Ishida, Y. Okamoto, J. Catal. 227 (2004) 523.
[9] J. Vakros, K. Bourikas, C. Kordulis, A. Lycourghiotis, J. Phys. Chem. B 107 (2003) 1804.
[10] J. Vakros, C. Kordulis, A. Lycourghiotis, Langmuir 18 (2002) 417.
[11] E.J.M. Hensen, P.J. Kooyman, Y. van de Meer, A.M. van de Kraan, V.H.J. de Beer, J.A.R. van Veen, R.A. van Santen, J. Catal. 199 (2001) 224.
[12] M. Sun, D. Nicosia, R. Prins, Catal. Today 86 (2003) 173.
[13] R. Cattaneo, F. Rota, R. Prins, J. Catal. 199 (2001) 318.
[14] T. Shimizu, K. Hiroshima, T. Honma, T. Mochizuki, M. Yamada, Catal. Today 45 (1998) 271.
[15] L. Medici, R. Prins, J. Catal. 163 (1996) 38.
[16] M. Sun, T. Burgi, R. Cattaneo, R. Prins, J. Catal. 197 (2001) 172.
[17] M. Sun, T. Burgi, R. Cattaneo, D. van Langeveld, R. Prins, J. Catal. 201 (2001) 258.
[18] M. Jian, R. Prins, J. Catal. 179 (1998) 18.
[19] H. Kraus, R. Prins, J. Catal. 170 (1997) 20.
[20] H.A. Therese, J.X. Li, U. Kolb, W. Tremel, Solid State Sci. 7 (2005) 67.
[21] H. Wei, Y. Wu, N. Lun, C. Hu, Mater. Sci. Eng. A 393 (2005) 80.
[22] B. Tang, L. Zhuo, J. Ge, J. Niu, Z. Shi, Inorg. Chem. 44 (2005) 2568.
[23] L. Ding, Z. Zhang, Y. Zheng, Z. Ring, J. Chen, Appl. Catal. A 301 (2006) 241.
[24] L. Qu, W. Zhang, P.J. Kooyman, R. Prins, J. Catal. 215 (2003) 7.
[25] M. Sun, P.J. Kooyman, R. Prins, J. Catal. 206 (2002) 368.
[26] S. Texier, G. Berhault, G. Pérot, V. Harlé, F. Diehl, J. Catal. 223 (2004) 404.

[27] M.P. De la Rosa, S. Texier, G. Berhault, A. Camacho, M.J. Yácaman, A. Mehta, S. Fuentes, J.A. Montoya, F. Murrieta, R.R. Chianelli, J. Catal. 225 (2004) 288.
[28] M.V. Landau, L. Vradman, M. Herskowitz, Y. Koltypin, A. Gedanken, J. Catal. 201 (2001) 22.
[29] D. Ferdous, A.K. Dalai, J. Adjaye, Appl. Catal. A 260 (2004) 153.
[30] C. Glasson, C. Geantet, M. Lacroix, F. Labruyere, P. Dufresne, J. Catal. 212 (2002) 76.
[31] E. Lecrenay, K. Sakanishi, I. Mochida, T. Suzuka, Appl. Catal. A 175 (1998) 237.
[32] G.M. Kumaran, S. Garg, K. Soni, V.V.D.N. Prasad, L.D. Sharma, G.M. Dhar, Energy Fuels 20 (2006) 1784.
[33] D. Li, T. Sato, M. Imamura, H. Shimada, A. Nishijima, J. Catal. 170 (1997) 357.
[34] L. Karakonstantis, H. Matralis, C. Kordulis, A. Lycourghiotis, J. Catal. 162 (1996) 306.
[35] K.V.R. Chary, G. Kishan, K.S. Lakshmi, K. Ramesh, Langmuir 16 (2000) 7192.
[36] J.W. Geus, in: G. Poncelet, P. Grange, P.A. Jacobs (Eds.), Preparation of Catalysts III, Elsevier, Amsterdam, 1983, p. 6.
[37] A.J. van Dillen, R.J.A.M. Terörde, D.J. Lensveld, J.W. Geus, K.P. de Jong, J. Catal. 216 (2003) 257.
[38] M. Sun, N. Xu, Y.W. Cao, J.N. Yao, E.G. Wang, J. Mater. Sci. Lett. 19 (2000) 1407.
[39] A. Hyvärinen, H. Lihavainen, A. Gaman, L. Vairila, H. Ojala, M. Kulmala, Y. Viisanen, J. Chem. Eng. Data 51 (2006) 255.
[40] O. Vasylkiv, Y. Sakka, Scripta Mater. 44 (2001) 2219.
[41] Z. Lu, S.M. Kanan, C.P. Tripp, J. Mater. Chem. 12 (2002) 983.
[42] Y. Zhai, S. Zhang, H. Pang, Mater. Lett. 61 (2007) 1863.
[43] A. Michailovski, F. Krumeich, G.R. Patzke, Mater. Res. Bull. 39 (2004) 887.
[44] S. Giri, S. Samanta, S. Maji, S. Ganguli, A. Bhaumik, J. Magn. Magn. Mater. 285 (2005) 296.
[45] Z. Sun, T. Zheng, Q. Bo, M. Du, W. Forsling, J. Colloid Interface Sci. 319 (2008) 247.
[46] Y. Shin, T.S. Zemanian, G.E. Fryxell, L. Wang, J. Liu, Microporous Mesoporous Mater. 37 (2000) 49.
[47] K.D. Dobson, A.J. McQuillan, Spectrochim. Acta Part A 55 (1999) 1395.
[48] Y. Mao, B.M. Fung, J. Colloid Interface Sci. 191 (1997) 216.
[49] H.E. Evans, W.H. Weinberg, J. Chem. Phys. 71 (1979) 4789.
[50] D. Nicosia, R. Prins, J. Catal. 229 (2005) 424.
[51] U. Usman, M. Takaki, T. Kubota, Y. Okamoto, Appl. Catal. A 286 (2005) 148.
[52] Y. Okamoto, Y. Arima, K. Nakai, S. Umeno, N. Katada, H. Yoshida, T. Tanaka, M. Yamada, Y. Akai, K. Segawa, A. Nishijima, H. Matsumoto, M. Niwa, T. Uchijima, Appl. Catal. A 170 (1998) 315.
[53] A. Benitez, J. Ramírez, A. Vazquez, D. Acosta, A. López Agudo, Appl. Catal. A 133 (1995) 103.
[54] J. Ramírez, P. Castillo, A. Benitez, A. Vazquez, D. Acosta, A. López Agudo, J. Catal. 158 (1996) 181.
[55] H. Wang, Y. Fan, G. Shi, Z. Liu, H. Liu, X.J. Bao, Catal. Today 125 (2007) 149.
[56] D. Ferdous, A.K. Dalai, J. Adjaye, L. Kotlyar, Appl. Catal. A 294 (2005) 80.
[57] J. Cruz, M. Avalos-Borja, R. López Cordero, M.A. Bañares, J.L.G. Fierro, J.M. Palacios, A. López Agudo, Appl. Catal. A 224 (2002) 97.